DTIC FILE COPY

(2)

AD-A192 156

REPORT DOCUMENTATION PAGE

1a. REPORT SECURITY CLASSIFICATION: Unclassified	1b. RESTRICTIVE MARKINGS
2a. SECURITY CLASSIFICATION AUTHORITY	3. DISTRIBUTION/AVAILABILITY OF REPORT: Approved for public release, distribution unlimited.
2b. DECLASSIFICATION/DOWNGRADING SCHEDULE	
4. PERFORMING ORGANIZATION REPORT NUMBER(S)	5. MONITORING ORGANIZATION REPORT NUMBER(S): AFOSR-TR- 88-0105
6a. NAME OF PERFORMING ORGANIZATION: Mechanical Engineering, University of Florida (6b. OFFICE SYMBOL (If applicable))	7a. NAME OF MONITORING ORGANIZATION: Air Force Office of Scientific Research/NA
6c. ADDRESS (City, State and ZIP Code): 237 MEB, University of Florida, Gainesville, FL 32611	7b. ADDRESS (City, State and ZIP Code): AFOSR/NA, Bolling AFB DC 20332-6448
8a. NAME OF FUNDING/SPONSORING ORGANIZATION: Air Force Office of Scientific Research (8b. OFFICE SYMBOL (If applicable): AFOSR/NA)	9. PROCUREMENT INSTRUMENT IDENTIFICATION NUMBER: AFOSR Grant 85-0113
8c. ADDRESS (City, State and ZIP Code): Building 410, Bolling AFB, DC 20332-6448	10. SOURCE OF FUNDING NOS.

PROGRAM ELEMENT NO.	PROJECT NO.	TASK NO.	WORK UNIT NO.
61102F	2308	A1	

11. TITLE (Include Security Classification): Pressure and Gas flow Gradients Behind Projectile During the Interior Ballistic Cycle

12. PERSONAL AUTHOR(S): E.C. Hansen and O.K. Heiney

13a. TYPE OF REPORT	13b. TIME COVERED	14. DATE OF REPORT (Yr., Mo., Day)	15. PAGE COUNT
Reprint	FROM _____ TO _____	1987 October 27	9

16. SUPPLEMENTARY NOTATION

17. COSATI CODES			18. SUBJECT TERMS (Continue on reverse if necessary and identify by block number)
FIELD	GROUP	SUB. GR.	Interior Ballistics, Gas Gradients.

19. ABSTRACT (Continue on reverse if necessary and identify by block number)

A very important factor in determining the projectile acceleration in a lumped parameter ballistic model is the relationship between the computed parameter, the space mean pressure, and the parameter defining the projectile motion, the pressure acting on the base of the projectile. The gradients of pressure and density from the breech to projectile were postulated to depend on the term, projectile acceleration times axial position. The model compared favorably with experimental measurements of downbore to chamber pressure ratios.

Keywords:

Presented at the Tenth International Symposium on Ballistics sponsored by the American Defense Preparedness Association on October 27, 1987.

DTIC ELECTE MAR 02 1988 S E D

20. DISTRIBUTION/AVAILABILITY OF ABSTRACT	21. ABSTRACT SECURITY CLASSIFICATION
UNCLASSIFIED/UNLIMITED [X] SAME AS RPT. [ ] DTIC USERS [ ]	Unclassified

22a. NAME OF RESPONSIBLE INDIVIDUAL	22b. TELEPHONE NUMBER (Include Area Code)	22c. OFFICE SYMBOL
Dr. Julian M. Tishkoff	202-767-0465	AFOSR/NA

DD FORM 1473, 83 APR — EDITION OF 1 JAN 73 IS OBSOLETE

Unclassified
SECURITY CLASSIFICATION OF THIS PAGE

PRESSURE AND GAS FLOW GRADIENTS BEHIND THE PROJECTILE DURING THE INTERIOR BALLISTIC CYCLE

E.C. Hansen
Mechanical Engineering
University of Florida
Gaiesville, FL 32611

O.K. Heiney
Rocketdyne Div.
Rockwell International Corp.
6633 Canoga Ave.
Canoga Park, CA 91303
D/522-BA26

A very important factor in determining the projectile acceleration in a lumped parameter ballistic model is the relationship between the computed parameter, the space mean pressure, and the parameter defining the projectile motion, the pressure acting on the base of the projectile. The gradients of pressure and density from the breech to projectile were postulated to depend on the term, projectile acceleration times axial position. The model compared favorably with experimental measurements of downbore to chamber pressure ratios.

INTRODUCTION

The techniques for analytically describing the pressure gradient which exists from the static conditions in the breech to the turbulent area directly behind the projectile have been one of the central problems of interior ballistics from the inception of the science, to the present day. The closed form interior ballistics of the 1940's generally used a constant factor pressure decrement, based on the propellant charge to projectile mass ratio. These factors were derived from an integral approach and applied incrementally. Although they were nowhere correct on a stepwise basis, in the aggregate they were effective and suitable for the closed form calculations of the time.

In England the approach used by Corner [Ref. 1] and Hunt-Hinds [Ref. 2] was that of a shot base pressure P_s to breech pressure ratio P_b relationship of

$$P_s = P_b/(1 + \tfrac{1}{2} C/M)$$

With a C/M = .5 this predicts

$$P_s = .8P_b$$

In the United States, the Hirschfelder approach [Ref. 3] used an average pressure P_{ave} expression of the form

$$P_{ave} = P_s \left(\frac{M + C/3}{M} \right)$$

which with a C/M = 0.5 predicts
$P_s = .87\ P_{ave}$ or in terms of P_b
$P_s = .76\ P_b$

Both approaches recognized that these approximations became increasingly less accurate as the charge to mass ratio increased above 0.5.

As computers became generally available in the early 1960's, other approaches and relationships were postulated for the lumped parameter interior ballistic formulations which were developed to model the interior ballistic process while

avoiding solving coupled partial differential equations. An approach used for many years by one of the authors [Ref. 4] postulated that the pressure differential from the breech to the base of the projectile could be expressed in terms of the velocity of the projectile, by means of "quasi-isentropic" approaches, that is:

$$\frac{P_s}{P_b} = \left[1 + \left(\frac{\gamma-1}{2}\right)\left(\frac{U_p^2}{\gamma gRT}\right)\right]^{-\gamma/\gamma-1}$$

or

$$\frac{P_s}{P_{ave}} = \left[1 + \left(\frac{\gamma-1}{2\phi}\right)\left(\frac{U_p^2}{\gamma gRT}\right)\right]^{-\gamma/\gamma-1}$$

with the value $U_p^2/\gamma gRT$ being the Mach number squared of the propellant combustion gases at the base of the projectile.

With a C/M = .5 this approach, when integrated, would give an overall effective P_s/P_b ratio in the .75 to .8 range similar to the old Corner and Hirschfelder approach.

However, as C/M values of very high performance gun systems started to approach and even exceed values of C/M = 1 the velocity pressure postulate was found to theoretically under predict experimental gun firing experience.

More specifically, as in-bore velocity Doppler radar systems became available in the early 1970's and laser based visar in-bore velocity systems in the mid 1970's, it was experimentally seen that substantially more ΔV was imparted to the projectile later in the ballistic cycle than predicted by the velocity based "quasi-isentropic" postulate.

Clearly a more accurate postulate was required. From 1985 to 1987 the Air Force Armament Laboratory sponsored and the Air Force Office of Scientific Research funded an effort at the University of Florida to study high velocity in-bore gas dynamics and generate a better postulate as to the mechanistic description of in-bore gas gradients.

The balance of this paper provides the results of the study and indicates that the in-bore pressure gradient is not driven by the velocity of the projectile but rather by the acceleration of the projectile.

PHYSICAL MECHANISMS CAUSING PRESSURE AND DENSITY GRADIENTS

The physical mechanism postulated to cause a pressure difference between the breech and projectile is the acceleration of the projectile. As the projectile accelerates, it produces a series of expansion waves behind it. The pressure drops from breech to projectile through these waves.

The ballistic cycle begins as combustion occurs within the chamber bounded by the breech, tube wall, and projectile and increases the pressure. Because the burning rate of the propellant increases with increased pressure, high pressures are quickly produced. These high pressures accelerate the projectile producing a series of exansion waves behind it. These wave accelerate the gases behind the projectile to the velocity of the projectile. They travel toward the breech, reflect, and return to the projectile distributing the velocities of the gases between the breech and the projectile.

As the projectile accelerates, the gases behind the projectile also accelerate. This acceleration produces a gradient of pressure, density, and temperature behind the projectile. Subsequently, the

pressure at the base of the projectile is lower than that at the breech.

The pressure drop is then governed by the acceleration of the piston. After the acceleration stops, the pressure drop from the stationary end of the cylinder to the moving piston goes to zero. In a typical ballistic system the acceleration begins low, it then increases rapidly to a peak and drops off with movement of the projectile. It would then be reasonable that the drop of pressure from breech to projectile would be dependent on the acceleration history of the recent past. The recent past would be defined as the time between formation of an expansion wave and when that wave has reflected and returned to the piston. Once the expansion wave has returned to the piston, its remaining effect is only to lower the pressure of the gas in the chamber.

EQUATIONS OF MOTION FOR UNSTEADY FLOWS

The breech to projectile gradients of pressure, density and temperature are gorverned by the conservation equations of mass, momentum and energy. One dimensional forms of these equations were solved using simplifying assumptions to determine analytical relationships between the projectile acceleration and the gradients. The equations of motion for a mixture of gas and solids are the conservation of mass and the conservation of momentum.

$$\frac{\partial}{\partial t}\left(\rho_{sl}\,(1-\nu') + \rho\nu'\right) +$$

$$\frac{\partial}{\partial x}\left(\rho_{sl}(1-\nu')\,u_{sl} + \rho\nu' u\right) = 0 \qquad (1)$$

$$\frac{\partial}{\partial t}\left(u_{sl}\,\rho_{sl}\,(1-\nu') + u\rho\nu'\right) +$$

$$\frac{\partial}{\partial x}\left(u_{sl}^2\rho_{sl}\,(1-\nu') + u^2\rho\nu'\right) = -\frac{\partial P}{\partial x} \qquad (2)$$

It was assumed that the velocity of the solids is related to the velocity of the gas by a constant ratio throughout the tube at any particular instant. No friction or heat transfer effects were included. The two equations were combined to give an equation which has a form similar to the unsteady Bernoulli equation.

$$\frac{\rho_{ml}}{\rho_m}\int_0^x \frac{\partial u}{\partial t}\,dx + \left(\frac{\rho_{ml}u^2}{\rho_m}\right)\frac{1}{2}\Big|_x =$$

$$-\int_{P_b}^{P_x}\frac{dP}{\rho_m} \qquad (3)$$

$$\rho_m = \rho_{sl}\,(1-\nu') + \rho\nu'$$

$$\rho_{ml} = \rho_{sl}\,(1-\nu')\,u_{sl}/u + \rho\nu'$$

The terms on the left hand side of Eqn. 3 are acceleration terms. The integrated acceleration produces the pressure difference from breech to projectile. The right hand side represents the pressure gradient produced by the acceleration.

Acceleration Term

The acceleration term was evaluated for solids and gases. A linear profile of velocity with distance was assumed for both the velocities of gas and solids. The velocity of the solids was assumed to lag that of the gas by the ratio u_{sl}/u. This approach was used because several different models including the XNOVA code [Ref. 5] indicated that the gas velocity profile was quite linear.

When the acceleration of the piston is zero, the linear velocity model seems to predict that the velocity past a point is always

decreasing. When $a_p > v^2/L$, the velocity past a point will increase with time. When $a_p < v^2/L$, the velocity past a point will decrease with time. This does not mean however, that the velocity of a particle is slowing down. As one follows a particle, it continues on at the same or greater velocity depending on the level of acceleration of the piston.

Assuming a linear velocity profile and integrating the acceleration side of equation 3 gave

$$\left[\frac{\rho_{ml}}{\rho_m}\frac{L\,a_p}{2} + \frac{u_p^2}{2}\left(\left(\frac{\rho_{ml}}{\rho_m}\right)^2 - \left(\frac{\rho_{ml}}{\rho_m}\right)\right)\right]\xi^2 = -\int_{P_b}^{P}\xi\,\frac{dP}{\rho_m} \qquad (4)$$

$$\text{or}\quad \frac{La_p^*}{2}\,\xi^2 = -\int_{P_b}^{P}\xi\,\frac{dP}{\rho_m} \qquad (5)$$

The most significant portion of the acceleration side is $L\,a_p/2$. The factor ρ_{ml}/ρ_m accounts for solids which are not accelerating as fast as the gas. The projectile velocity squared portion of the acceleration side will always have a minus sign in front of it because ρ_{ml}/ρ_m is always less than 1. When there are no longer any solids, ρ_{ml}/ρ_m goes to 1 and the entire acceleration term goes to $L\,a_p/2$.

The ratio ρ_{ml}/ρ_m is determined knowing the porosity, the gas density, and u_{sl}/u.

u_{sl}/u was estimated as a constant along the barrel at any instant in time. It was assumed to change with time. The ratio of average acceleration of the solids over the average acceleration of the gas was assumed to be equal to u_{sl}/u. The drag force on the cylindrical grain was assumed proportional to $(u-u_{sl})^2$ and equal to the acceleration of the grain times its mass.

u_{sl}/u was solved for as a function of a nondimensional acceleration number, Fa. Fa has been formulated to be a function of the easily determined parameters.

$$Fa = \frac{2C_D\rho U^2}{3\pi r_o \rho'_{sl}\, a_p}$$

$$\frac{u_{sl}}{u} = 1 + \frac{1}{2Fa}\left(1 - \sqrt{4\,Fa + 1}\right) \qquad (6)$$

The assumption of a linear velocity profile was tested using an inviscid computer model of gas flow in a tube between breech and projectile. The projectile was driven by estimates of accelerations from experimental shots 536 and 571 which will be discussed later. The ratio of the integrated particle acceleration (left hand side of equation 3) divided by $a_p\,L/2$ was plotted against time in Figures 1 and 2. If the velocity profile was linear, the ratio would be 1. In Figure 1 the ratio is 0.98 during the last 70% of the time. This indicates that the integrated acceleration estimate of $a_p\,L/2$ is 2% high. Figure 2 is for a case with a 30% higher peak pressure. This higher pressure causes increased acceleration. This increased acceleration rate is the probable cause of the hump in Figure 2 that starts at 0.002 seconds. The peak of the hump, 1.07, indicates that the integrated acceleration estimate of $a_p\,L/2$ is 7% low.

Pressure Gradient Term

The pressure gradient term was evalated for the two cases of gas only and of gas and solids. The pressure was integrated by assuming an isentropic relationship between pressure and density.

The integration of the gas only

case stated in terms of breech temperature and density directly yielded equation 7a.

$$\frac{P_\xi}{P_b} = \left(1 - \frac{(\gamma-1)(1-\rho_b\eta)\, L\, a_p\, \xi^2}{2\gamma\, R\, T_b}\right)^{\frac{\gamma}{\gamma-1}} \quad (7a)$$

When stated in terms of breech pressure and density it yielded

$$\frac{P_\xi}{P_b} = \left(1 - \frac{(\gamma-1)\, \rho_b\, L\, a_p\, \xi^2}{2\gamma\, P_b}\right)^{\frac{\gamma}{\gamma-1}} \quad (7b)$$

The gas and solids case was integrated using a linearized form of the term $(P/P_b)^{(1/\gamma)}$. The equation was stated in terms of breech temperature and density

$$\frac{P_\xi}{P_b} = 1 + \gamma\left(\frac{\rho_{sl}(1/\nu'-1)}{\rho_b} + 1\right)^* \left[\exp\left(\frac{-\nu'(1-\rho_b\eta)La_p\,\xi^2}{2\gamma RT_b}\right) - 1\right] \quad (8a)$$

It was also stated in terms of breech pressure and density.

$$\frac{P_\xi}{P_b} = 1 + \gamma\left(\frac{\rho_{sl}(1/\nu'-1)}{\rho_b} + 1\right)^* \left[\exp\left(\frac{-\nu'\,\rho_b La_p\,\xi^2}{2\gamma P_b}\right) - 1\right] \quad (8b)$$

The multiplier term $(\rho_{sl}\,(1/\nu' - 1)/\rho_b + 1)$ can greatly increase the pressure drop from breech to projectile over the gas only case. This is because the large forces are needed to accelerate the solids which have a density much greater than the gases. The average pressure can be determined by integration of a series expansion of 8b.

$$\frac{P_{ave}}{P_b} = 1 + K_1\left(-\frac{K_2}{3} + \frac{K_2^2}{10} - \frac{K_2^3}{42} + \frac{K_2^4}{216} - \frac{K_2^5}{1320}\right) \quad (9)$$

$$K_1 = \left(\frac{\rho_{sl}\,(1/\nu'-1)}{\rho_b} + 1\right)\gamma$$

$$K_2 = \frac{\nu'(1-\rho\,\eta)La^*}{2\gamma RT_b}$$

Kinetic Energy in the Gases

The ratio of kinetic energy in the gas solid mixture to the kinetic energy of the same mass moving at the projectile velocity is $1/\delta$. δ was obtained using a linear velocity distribution and a parabolic density distribution obtained from the pressure distribution of Eqn. 8.

$$\delta = 3\,\frac{\frac{\rho_{sl}(1-\nu')}{\rho_b\nu'} + \left(1 - \frac{\rho_s}{3\rho_b}\right)}{\frac{\rho_{sl}(1-\nu')}{\rho_b\nu'}\left(\frac{u_s}{u}\right)^2 + \left(1 - \frac{3\rho_s}{5\rho_b}\right)} \quad (10)$$

The case of gas only

$$\delta = \frac{3\left(1 - \frac{\rho_s}{3\rho_b}\right)}{\left(1 - \frac{3}{5}\,\frac{\rho_s}{\rho_b}\right)} \quad (11)$$

COMPARISIONS OF ANALYTICAL MODEL WITH EXPERIMENTAL DATA

The equations just described in were compared with experimental data

from Eglin AFB for firings with muzzle velocities of 1000 m/s. Comparisons were also made with computer modelled predictions obtained from Eglin AFB and the Ballistics Research Lab. The experimental data came from two series of shots of a 30 mm aircraft cannon. Each series consisted of four shots. These runs were evaluated by shifting the time scales to make the peak pressures coincide and then comparing the measured pressures in time. The two pressure time traces which best matched each other were then used as the standard data for each series.

Each set of data consisted of time and for pressure readings. The first reading was called the chamber pressure reading. It was not taken at the breech but just in front of the initial position of the rotating band. The three other readings were taken at three downbore locations.

The data in a nondimensional form were used for the comparison with analytical equations (7 and 8). The pressures at the three downbore locations were normalized by the chamber pressure reading. The resulting pressure ratio was less than 1 because the downstream pressures were always lower than the chamber pressure.

The analytical pressure ratio was determined using equation 8 to find the downbore pressure with respect to the breech pressure for both the chamber location and the downbore location. Values of the variables in equation 8 were obtained from an interior ballistics program of Heiney [Ref 4]. The variables needed were average porosity, breech density and pressure, projectile acceleration, and breech to projectile length. The analytical pressure ratio was determined as a function of time for each downbore pressure tap location beginning from the time that each tap was passed by the projectile.

The results are quite encouraging. Comparisons with the 536 experimental data is shown in Figures 3-5. The experimental data is the jagged line. The other two lines are the results of calculations from equation 8 with the upper line being a gas only calculation and the lower line being the calculation when solids are included. At 1700 microseconds in Figure 3 one can see that the solids theory agrees quite well with the data.

At a later time of 2500 microseconds in Figure 4 the gas only theory seems to be a better estimate than that of the solids. This is probably due to the fact that the solids do not follow directly behind the projectile but lag it. The ξ squared term in equation 8, causes the majority of the pressure drop to occur in the 30% of the length just behind the projectile. If the solids concentration is very low in this region, the pressure will drop less and will better follow the gas only theory.

The last figure in the 536 series is Figure 5. It shows good agreement between theory and experiment for either gas only or gas and solids. The two theoretical lines are very close because at 3000 microseconds there are very few solids left.

Comparisons of 571 experimental data with theory are shown in Figures 6-8. This shot had a muzzle velocity 7% higher than the previous 536 shot. This was produced by a thinner grain web thickness. Figure 6 shows the pressure ratio for downbore tap 2. Burning has occurred more quickly and few solids remain so that the gas and solids lines are very close. Predicted pressures are lower than those measured. One explanation may be lack of time for the velocity profile to become linear after the time of peak

pressure.

Figure 7 shows quite good agreement with the experimental data over the last half of the time of the run. Figure 8 shows a pressure ratio higher than the data. This may be related to the hump in acceleration ratio shown in Figure 2

Two higher speed cases were compared with theory. Experimental data was not available for either of these. However, computer predictions were available using two different codes which model the flow of both solid and gas as the solids burn.

The first case had a 1400 m/s muzzle velocity. Combustion was complete and gas only theory was compared. Pressure at the projectile base over pressure at the breech was compared when the projectile was at the muzzle. The computer prediction of the pressure ratio was 0.707 and the pressure ratio of the theory of this work was 0.665.

The second case was a large diameter round with a 1450 m/s muzzle velocity. Combustion was complete and the pressure ratios was compared when the projectile was at the muzzle. The computer prediction of the pressure ratio was 0.731 and the pressure ratio of the theory of this work was 0.747.

In both of these cases the theory matched the computer predictions well. The Mach number of the gases behind the projectile in both of the last two cases is near 1.5 indicating that the flow was supersonic.

SUMMARY

The gradient in pressure and density from breech to projectile was postulated to be caused by the acceleration of the gases behind the projectile. The major governing parameter was the projectile acceleration times the axial position of the projectile.

ACKNOWLEDGEMENTS

Research sponsored by the Air Force Office of Scientific Research, Air Force Systems Command, USAF, under Grant Number AFOSR 85-0113. The U.S. Government is authorized to reproduce and distribute reprints for Governmental purposes not withstanding any copyright notation thereon.

NOMENCLATURE

a_p	-	acceleration of projectile
a_p*	-	adjusted acceleration
C	-	change mass
Fa	-	acceleration number
L	-	distance x between breech and projectile
M	-	projectile mass
P	-	pressure
P_{ave}	-	average chamber pressure
R	-	gas constant
t	-	time
T	-	temperature
u	-	velocity of gas
u_p	-	velocity of projectile
	-	kinetic energy of mass of gas at u_p/kinetic energy of gas
γ	-	specific heat ratio C_p/C_v
η	-	covolume
ν'	-	porosity
ξ	-	x/L
ρ_m	-	average density
ρ_{m1}	-	density times velocity average
ρ_{m2}	-	density times velocity squared average
	-	propellant grain density
ρ_{s1}'	-	density of a grain including gas within

perforation

ϕ - space mean factor

Subscripts

b - breech

s - projectile base, shot

sl - solids

x - axial position beginning at breech

REFERENCES

1. Corner J., "Theory of the Interior Ballistics of Guns" John Wiley, 1950.

2. Hunt, F.R., and Hinds, G.H., "Internal Ballistics" HMSO London, 1951.

3. Hirschfelder, J.O., Et al, "Interior Ballistics" NDRC Report A-142, 1943.

4. Heiney, O.K., and West, R.J., "Interior Ballistics, Muzzle Flash and Gas Gradients of Aircraft Cannon", AFATL-TR-76-34, 1976.

5. Gough, P.S., 'XNOVA -An Express Version of the NOVA Code", Contract Report N00174-82-M-8048, Naval Ordinance Station, Indian Head, Maryland, November 1983.

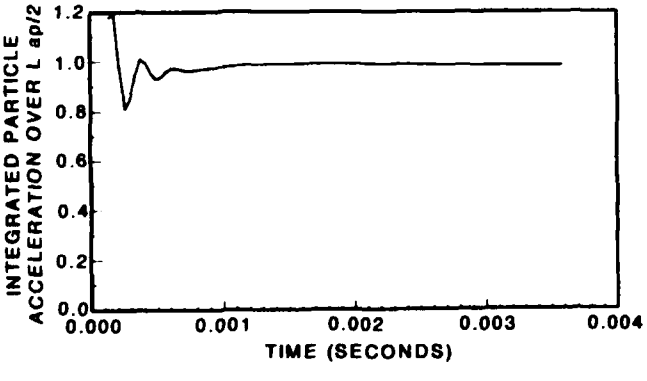

Figure 1. Instantaneous Particle Acceleration Integrated from Breech to Projectile Over L ap/2 Calculated Using Inviscid Theory of a Compressible Gas Using Acceleration of the Projectile from Shot 536.

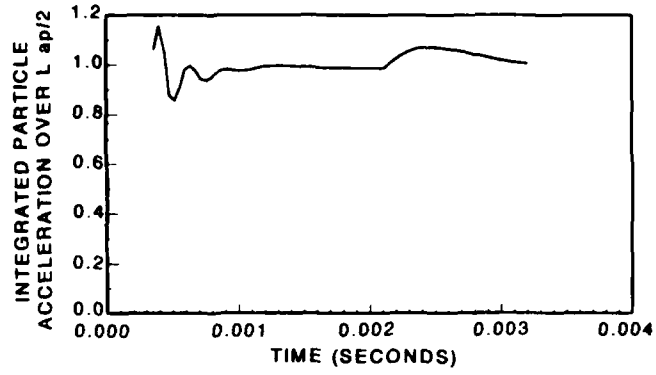

Figure 2. Instantaneous Particle Acceleration Integrated from Breech to Projectile Over L ap/2 Calculated Using Inviscid Theory of a Compressible Gas Using Acceleration of the Projectile from Shot 571.

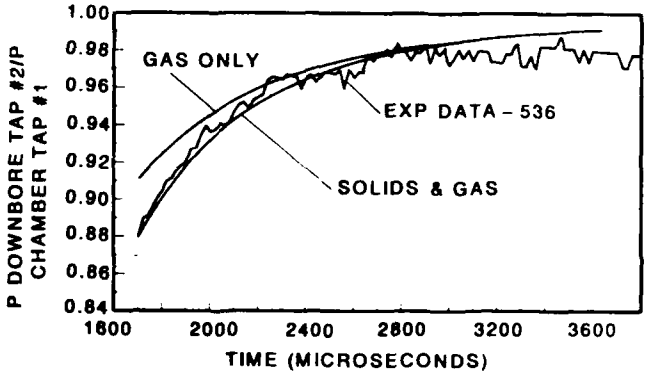

Figure 3. Pressure at Downbore Tap #2 Over Pressure at Chamber Tap #1 as a Function of Time.

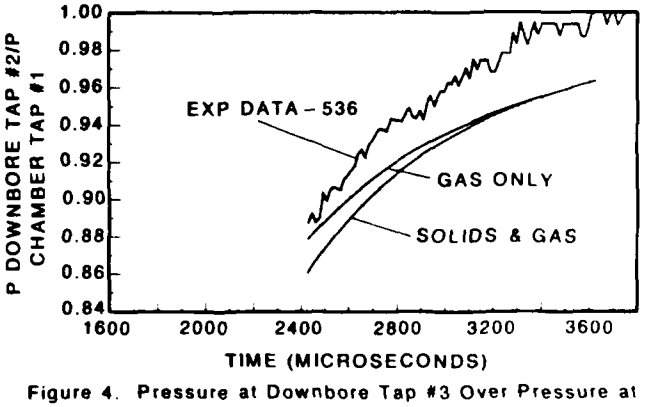

Figure 4. Pressure at Downbore Tap #3 Over Pressure at Chamber Tap #1 as a Function of Time.

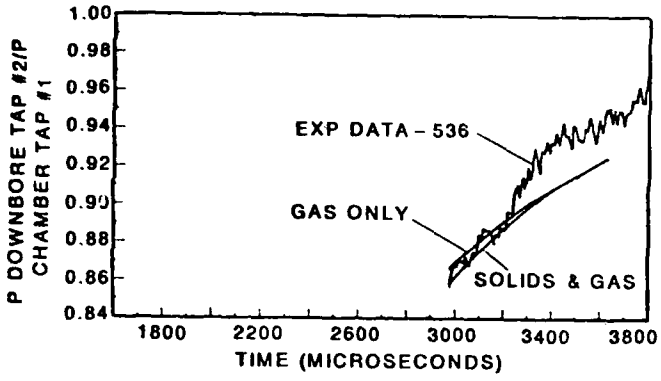

Figure 5. Pressure at Downbore Tap #4 Over Pressure at Chamber Tap #1 as a Function of Time.

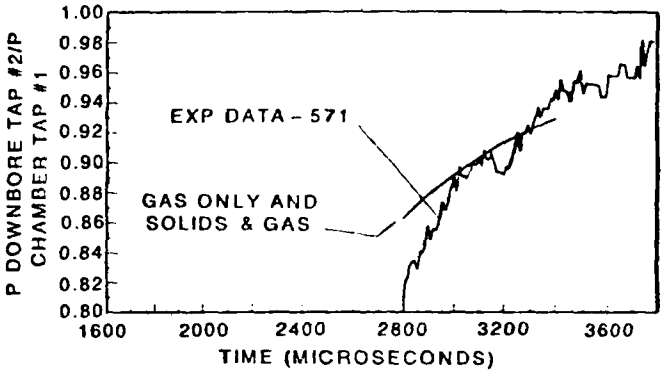

Figure 8. Pressure at Downbore Tap #4 Over Pressure at Chamber Tap #1 as a Function of Time.

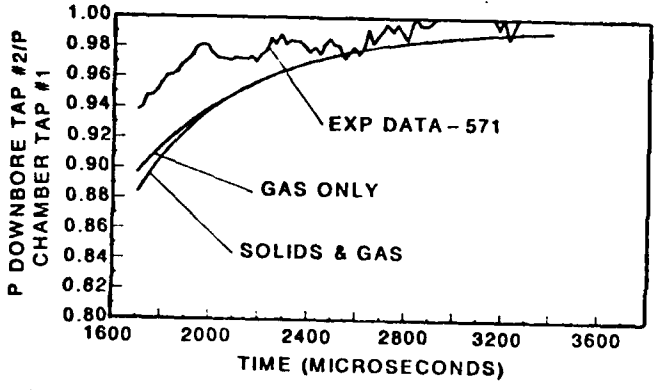

Figure 6. Pressure at Downbore Tap #2 Over Pressure at Chamber Tap #1 as a Function of Time.

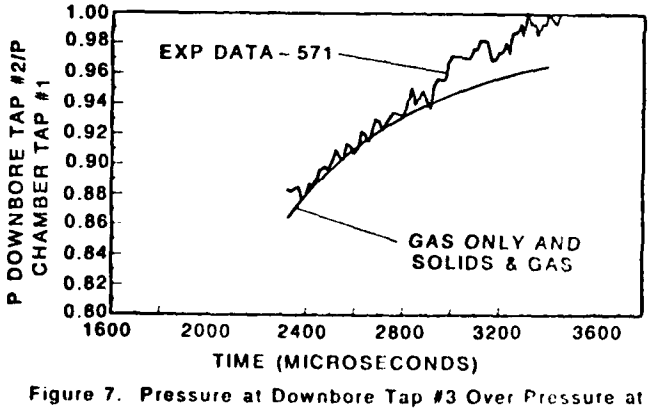

Figure 7. Pressure at Downbore Tap #3 Over Pressure at Chamber Tap #1 as a Function of Time.